Near Surface Geophysics, 2016, **14**, xxx-xxx doi: 10.3997/1873-0604.2016012

Usage of directional common image gathers for shallow seismic source localization

Ariel Lellouch* and Moshe Reshef

Tel Aviv University, Department of Geophysics, Tel-Aviv 69978 Israel

Received June 2015, revision accepted December 2015

ABSTRACT

Accurate localization of shallow subsurface seismic events recorded by an array of receivers might be challenging given the near-surface complexity and its inadequate spatial sampling, low velocities, and limited frequency content. A novel approach that performs a joint localization and velocity analysis is presented. In this study, we utilize non-conventional migrated common image gathers as a tool for velocity and location analysis, based on the diffractive nature of the source. Only when the correct velocity model is used energy from all receivers is coherently focused at the true subsurface location. However, if the used model or CIG location is wrong, the migrated event does not have a flat moveout. The effectiveness of this technique is greatly improved by the use of vertical arrays of receivers. Through synthetic and real data examples, we show the usefulness of the method in a fully automatic workflow.

INTRODUCTION

The development of an accurate, automatic, and fast method for localization of shallow seismic events could be used for a broad range of applications, such as underground intrusion/extrusion detection, monitoring of crack or faults developing in critical infrastructure, and guidance of search and rescue teams in catastrophes. For such a method to be effective, its error must be small in all directions, and the localization has to work from standoff, i.e., without receivers directly above the target. The reason is that, in some cases, particularly when monitoring underground intrusion/excursion, covering the entire area of interest with receivers might be impractical (for example, near a border) or at best very costly. Reaching those goals in the shallow subsurface might be very challenging due to its high heterogeneity and its inadequate spatial sampling, low velocities, and limited frequency content.

Localization of seismic events is a conventional procedure in seismology and micro-seismic applications (Earle and Shearer 1994; Bai and Kennett 2000). However, most of the standard methods use a picking-based procedure (Maxwell and Urbancic 2001), which is bound to, given the poor quality of signals in the shallow subsurface, induce errors. Poor signal quality might as well delay the process if manual picking is required. Furthermore, most of these methods assume that the velocity model is known (Bardainne and Gaucher 2010) and do not deal with analyzing its quality or updating it – which may be a problematic assumption when dealing with the complex shallow subsurface section and its relatively limited prior knowledge one may expect to have.

* lellouch@gmail.com

In the following, we propose an imaging-based method for source localization in which the source is the imaging target, i.e., ideally, a point in space. By first migrating the data into conceptually ideal pre-stack common image gathers (CIGs) using a one-way Kirchhoff depth migration, one has the ability to conduct a velocity analysis procedure jointly with the source's localization, which is in fact a form of diffraction imaging. Such an analysis can be a useful tool in estimating the quality of the used velocity model as well as possibly lead to its updating. In addition to the effectiveness of this novel method for interval velocity analysis, we show the necessity of a vertical acquisition geometry.

PREFERRED CIG PARAMETERS AND ANALYSIS

The large variety of Kirchhoff pre-stack depth migration (PSDMs) implementations allows for different choices of CIG parameters on which to perform the velocity analysis, such as acquisition offset, imaging offset, scattering angle and horizontal wavenumber (Biondi 2006). In any choice of parameters, a certain flatness optimization criterion is applied. Although most CIGs are usually presented as a function of a single parameter, usually acquisition offset or scattering angle, a migration velocity analysis (MVA) using only a single parameter might have questionable validity particularly in complex areas (Reshef and Rüger 2008) due to its inability to utilize all subsurface structural parameters used for PSDM.

Mapping surface coordinates into the subsurface depth image domain, known as the local angle domain (LAD), is performed using ray tracing (Koren and Ravve 2011; Ravve and Koren 2011). Setting aside depth, the pre-stack gathers contain two and four parameters for 2D and 3D applications, respectively. For the 2D case, these parameters are the structural and scattering dip angles

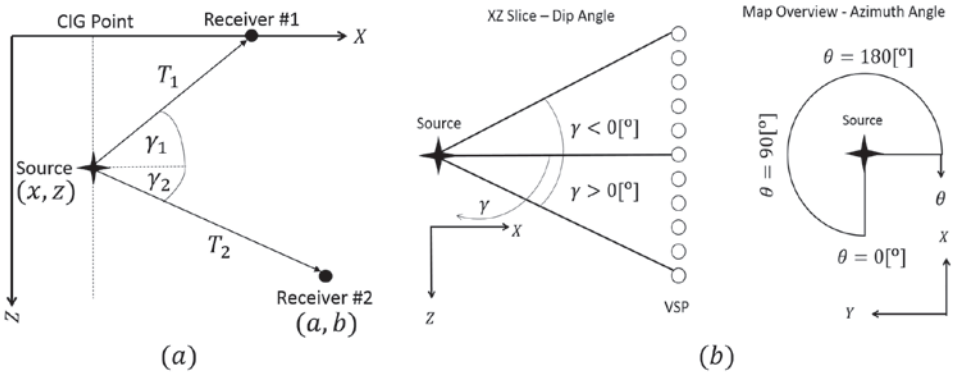

Figure 1 (a) Example of ray paths in 2D and (b) definition of dip and azimuth angles for a general (Vertical + Surface) 3D acquisition geometry.

(Reshef and Rüger 2008), whereas for a 3D case, the structural and scattering azimuth angles are added (Koren and Ravve 2011). However, since diffractions do not have a preferred spatial orientation, they can be represented by a single ray path connecting depth image point and receiver location (Reshef *et al.* 2012). Therefore, if velocity analysis is conducted on diffracted events, only one (in 2D) and two (in 3D) angles are needed for the CIGs. These angles' definition is shown in Figure 1. The common use of the local angle domain is with conventional surface seismic data where the subsurface reflections are the imaging target. However, the usage of these angles as the CIGs analysis parameters for diffraction imaging is particularly advantageous as they maintain the diffraction's omnidirectional radiation pattern and allow for a better directional analysis that is not affected by acquisition footprints. Furthermore, the usage of receivers in a vertically positioned configuration would provide larger dip angle coverage compared with standard surface acquisition.

Let us now describe the analytical expressions for dip angle gathers built in a 2D case of constant acoustic velocity model. In Fig.1 (left), we see a source at $\{x, z\}$ and a receiver at $\{a, b\}$. The dip angle is defined as the takeoff angle of the ray connecting source and receiver and is denoted by γ in the figure. The dip angle is negative if it is above the horizon and positive if it is below it. Without loss of generality, we will solve for $b > z$ (receivers above the source) and extend the solution at the end of the development. Geometrically, we see that

$$\alpha = x + \frac{b-z}{\tan(\gamma)} \tag{1}$$

$$t = \frac{b-z}{v\sin(\gamma)} \tag{2}$$

with τ being the source–receiver travel time in a constant velocity medium of velocity v. Those equations are undefined if $\gamma = 0$, but since this is a purely mathematical artefact, we will not deal with it in the development. The migration process, which purpose is to estimate the source location given the receiver location (α, b), source–receiver travel time τ, and migration velocity v_m, consists of solving the following equations:

$$x = \alpha - v_m \tau \cdot \cos(\gamma) \tag{3}$$

$$z = b - v_m \tau \cdot \sin(\gamma) \tag{4}$$

In order to do that, one has to choose the location x in which the CIG will be built. After choosing it, equation (3) can be used to estimate the dip angle γ. This angle can then be used to calculate the depth z of the migrated event using equation (4). However, as shown in equation (3), two opposite values of γ are possible. This dual possible choice of dip angle will yield two possible migrated depths z, symmetrical with respect to b, i.e., one above it and one below it.

Now, lets us assume a point diffractor at $\{x_0, z_0\}$ whose dip angle to the receiver is ξ. According to equations (1) and (2), its response in the data is

$$\alpha = x_0 + \frac{b-z_0}{\tan(\xi)} \tag{5}$$

$$\tau = \frac{b-z_0}{v\sin(\xi)} \tag{6}$$

Now, let us assume that not a single receiver exists at depth b but an infinite number of them, all at the same level, so as that every ray starting at the source location with dip angle ξ reaches one of the receivers. Under this assumption, the migrated image of the diffractive event is (equations (3) and (4))

$$x = x_0 + \frac{b-z_0}{\tan(\xi)} - \frac{v_m(b-z_0)\cos(\gamma)}{v\sin(\xi)} \tag{7}$$

$$z = b - \frac{v_m(b-z_0)\sin(\gamma)}{v\sin(\xi)} \tag{8}$$

We want to eliminate ξ as it is unknown. Solving equation (7) and substituting $\sin(\xi)$ in (8) yields, for the general case, the following:

$$z = b \pm \frac{v_m(b-z_0)(1+D^2)\sin(\gamma)}{-v_m D\cos(\gamma) + \sqrt{(1+D^2)v^2 - v_m{}^2\cos^2(\gamma)}}, D = \frac{x-x_0}{b-z_0} \tag{9}$$

The two possible opposite values of γ yield, as expected, two possible migrated depths. As one can see, if the image is constructed at the correct location ($x = x_0$ and thus $D = 0$) and using the correctly velocity ($v_m = v$) the imaged depth is either $z = z_0$ (the correct depth) or $z = 2b - z_0$ (a spurious solution), depending on whether γ is chosen to be positive or negative. This can be explained by the symmetry around the axis of the receivers' depth level (b). This equation (9) is true for both positive and negative γ, whereas the sign choice that yields the true solution alternates between them. Since we have no way of determining the true depth, we chose to keep the equation in this compact formulation.

Let us now look at a case of a surface line of receivers $(b = 0)$, in a constant velocity medium of 600 m/s and with a source at a depth of 15 m. For this example, we still assume an infinite line of receivers and only show a certain dip range of interest. Since the migrated event cannot be above surface level, there will be only one possible migrated depth. In Fig.2, we show the dependence of the dip angle gathers on the migration velocity and imaging point. Only if both are correct that the migrated event's moveout will be flat, as expected from equation (9). The distinctive non-flat moveout obtained otherwise is indicative and can also be used a basis for velocity/location analysis.

However, in practical scenarios, we have receivers in a vertical configuration and not as infinite setups at given levels. Therefore, the dip angle gather built from a vertical array configuration is a combination of different solutions of equation (9) using different values of *b*. For each receiver depth, two different migrated depths are possible, as previously explained. Since there is only a single receiver at depth *b*, we need to estimate the dip angle γ to which the recorded trace will be mapped. In constant velocity cases, this can be done geometrically through equation (3). In more complex velocity models, we use a ray tracing procedure. By shooting rays from the subsurface CIG point, we control the dip angle γ of the

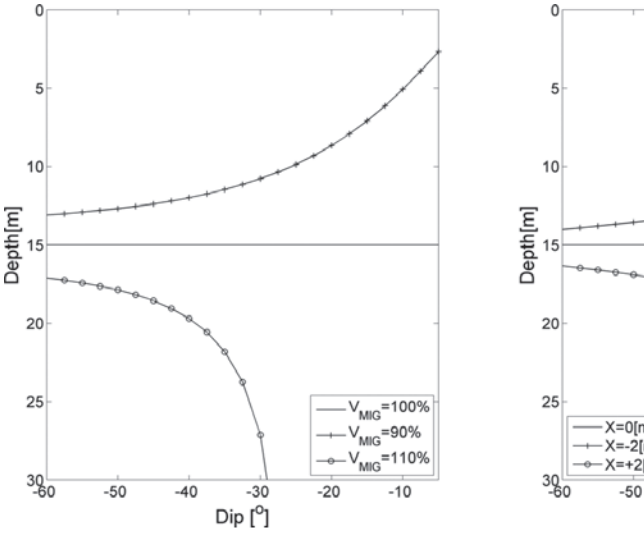

Figure 2 Dip angle gathers derived from equation 9. The gathers are shown for (a) different migration velocities and (b) different imaging locations. When the velocity or imaging location is wrong, the events' moveout is not flat.

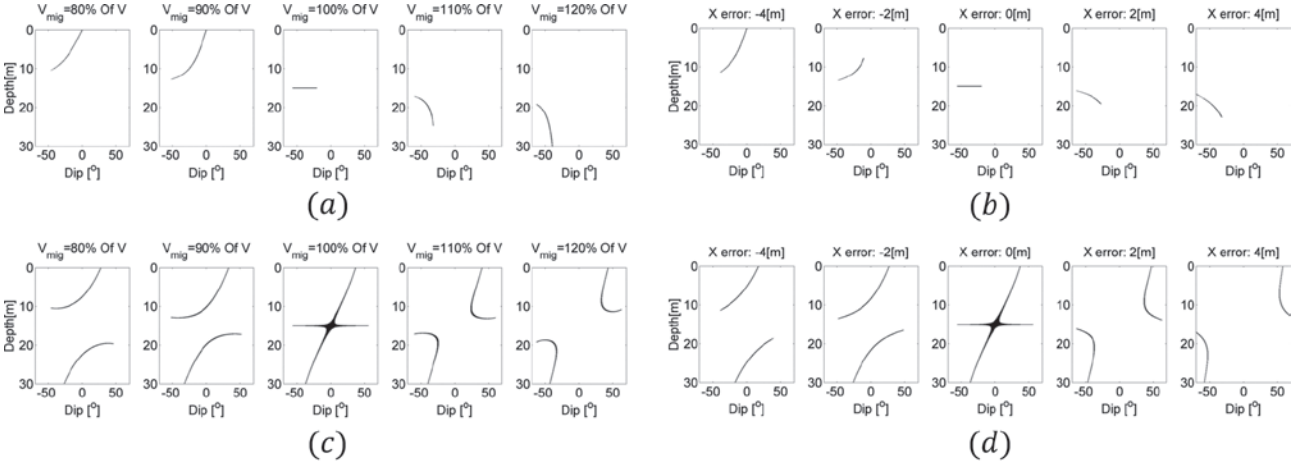

Figure 3 Analytic examples of dip angle gathers analysis. (a) Surface data migrated at the correct CIG with different velocities. (b) Surface data migrated at different CIG with the correct velocity. (c) Vertical data migrated at the correct CIG with different velocities (d) Vertical data migrated at different CIG with the correct velocity. We can see the high sensitivity to velocity and imaging location errors.

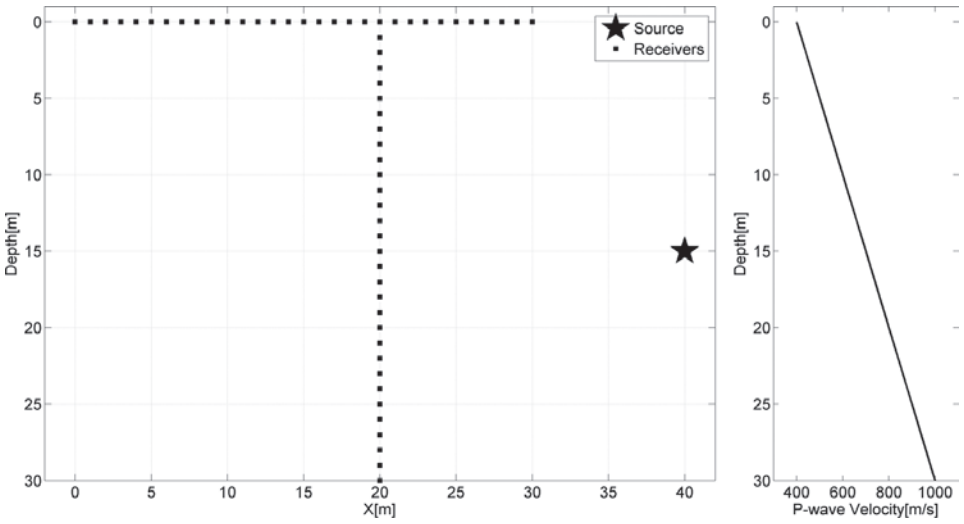

Figure 4 A synthetic 2D example scenario. The velocity model is a 1D gradient without lateral variation and a constant V_p / V_s ratio of $\sqrt{3}$.

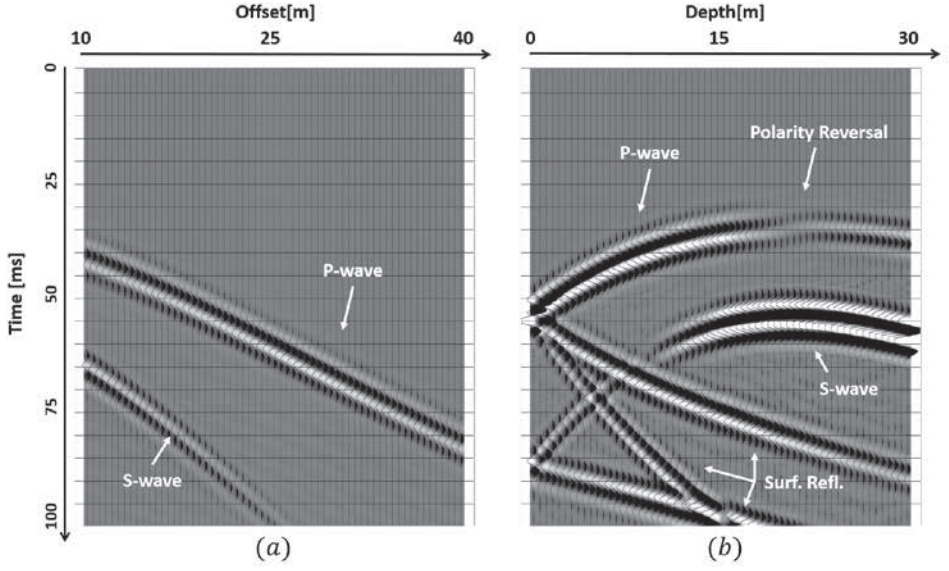

Figure 5 Synthetic data generated from the scenario described in Figure 4: (a) surface data sorted by X distance (offset) from the source and (b) vertical data sorted by receiver's depth. The different events are denoted by white arrows. Note the polarity reversal in the P-wave arrival in (b), which occurs at a depth of ~20[m] and the free surface reflections ("Surf. Refl.").

rays and can calculate their travel time τ to each of the receivers, given a migration velocity model.

Let us examine (Fig. 3) gathers derived from a simple example of a combination of surface and vertically positioned receivers in a constant velocity acoustic medium of 600 m/s. In this 2D scenario, a source at 15 m depth is recorded by a vertical array 10 m away and ranging in depths of 0 m–30 m as well as a surface line in offsets (distance along the surface) of 10 m–40 m. This scenario is representative of a standoff acquisition setup, whose importance was explained in the introduction. The surface data gathers look like standard MVA gathers, displaying upward-bending moveouts when velocity is too low and downward-bending moveouts when it is too high. On the opposite, the moveouts of events displayed in gathers built from vertically positioned receivers are very complex. At the correct velocity and location, there is a flat event at the true source depth, but it is accompanied by additional "tails" of dip-varying depth. This is readily explained by the analysis of equation (9), in which the concept of spurious migrated depth was introduced. As shown, the additional solution is a mirror image of the true one with respect to the receivers' level as axis of symmetry. Since for this vertical configuration the gather is built from receivers at different depth levels, each receiver yields a spurious solution at a different depth. As a result, for the true solution, the event will be migrated to the same depth for all dip angles, yielding the flat moveout part in the gather. In contrary, for the spurious solution, the source will be migrated to different depths at different dip angles, creating the unique "tails" of the moveout. It is also important to note the superior vertical setup coverage in terms of dip angles, despite the fact that vertical and surface receivers cover the same total distance of 30 m. This is an important conclusion, true as long as localization is conducted from standoff, and which will lead us to the usage of vertically positioned receivers in the next parts of this study.

For 3D acquisition geometries, the process of mapping seismic data into the angle domain for a single CIG is similar. Instead of a dip angle gather, the result is a 3D cube whose dimensions are $\{depth, dip, azimuth\}$. Different gathers can be obtained from summation along the dip or azimuth dimensions (Dafni and Reshef 2012).

THE USE OF DIP ANGLE CIGS FOR INTERVAL VELOCITY ANALYSIS

The use of generated dip angle gathers (either from working in a 2D scenario or after summation over azimuth angles) may be very convenient for velocity analysis. Moveouts of migrated events will be flat only at the true CIG point and if the correct velocity model is used. If this is not the case, they will, as we have shown, display a distinct behaviour that diverges from flatness (see also Bai *et al.* 2011). Since the subsurface is usually more complex in its depth variations than its lateral ones, the usage of dip angle gathers is preferable for interval velocity analysis as it will be more sensitive to the velocity profile in depth. The previously introduced usage of vertical receivers yields a very narrow azimuthal range and therefore further anchors the choice of analyzing dip angle gathers.

Due to the complexity of the velocity model and the usage of a single uncontrolled source as input data, the possibilities of updating the velocity model and detecting local anomalies are limited. In other words, had the problem been formulated as an inversion one, it would have been strongly underdetermined, thus ruling out tomography-type procedures. On the other hand, due to the strong variation of the velocity model, any attempt to use an effective, constant velocity is bound to fail, and no single velocity would be able to account for the strong depth variations, particularly when using vertical receivers. Therefore, we suggest starting with a certain good initial interval velocity model followed by applying bulk shifts (percentage change of the entire model) to it. This, despite being limited in updating local anomalies in the model, seems like the only practical approach to the problem and will still allow for first-order corrections to the initial model.

Let us move to a synthetic example. The scenario is described in Fig. 4 and consists of a linear depth-dependent velocity model without lateral changes and constant $\frac{V_P}{V_S}$ and density. A source is excited at 15 m depth and recorded from standoff by a combination of surface and vertical receivers, each covering a total distance of 30 m. The synthetic data, which are generated by a 3D spectral elements code for an elastic isotropic medium (Komatitsch and Tromp 1999) and emulating a uniaxial (Z) geophone recording a uniaxial (X) force source, i.e., towards the receivers position, are shown in Figure 5.

By using a ray tracing procedure from the subsurface image point to the receivers, a one-way Kirchhoff PSDM is performed to generate dip angle gathers. As explained, the process consists of shooting rays at known dip angles from each subsurface imaging point. For each ray reaching a receiver, we migrate the relevant trace to the dip angle of the ray using its calculated travel time. Repeating this process for all possible depth points of a given CIG yields a dip angle gather. For practical reasons, we elect to utilize the first arrivals of the P-waves only. Dip angle gathers built from surface data (containing offsets of 10 m–40 m) are shown in Figure 6 and show the dip angle gathers' sensitivity to the used velocity model.

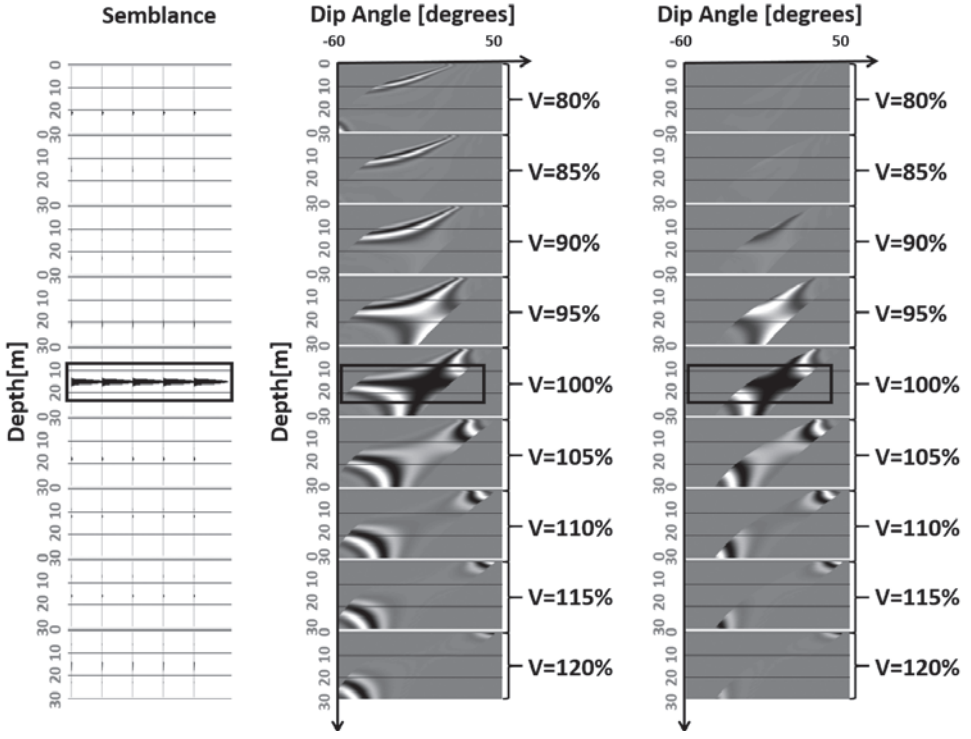

Figure 6 (Left) Semblance trace of the gathers in (middle) calculated with a 1-m window. The semblance trace (between 0 and 1) is repeated five times. (Middle) Dip angle gathers built from surface data only (using offsets of 10 m–40 m). The event's moveout is flat at the correct velocity, whereas for a low velocity, it is upward-bending and shallow and for a high velocity downward-bending and deep. (Right) Dip angle gathers built with surface data using offsets of 20 m–40 m. Those gathers are hardly usable due to the inability to discern the moveout of the event when wrong velocities are used and during due to narrow dip angle coverage.

The moveout of the migrated events for the negative dips resembles conventional MVA, as we saw in Figure 3: upward bending for too low velocity and downward-bending for too high. However, for positive dips, we see the uniquely shaped moveouts previously associated with vertical acquisition setups. The reason is that the strong velocity gradient bends the rays in such a way that even those starting, from a certain depth point, directed to below the horizon (positive dip) will reach the surface within the acquisition offset range. Therefore, the spurious migrated depth issue rises again. There are two possible ray paths with the same travel time, reaching the same surface receiver, in a given CIG point. One changes from positive to negative dip in its course, and the the second one stays negative for the entire path. However, since those rays emerge at different depths in the CIG, a spurious migrated event will be present in the gather. Nonetheless, the spurious depth is different for every dip, as was for the vertical acqui-

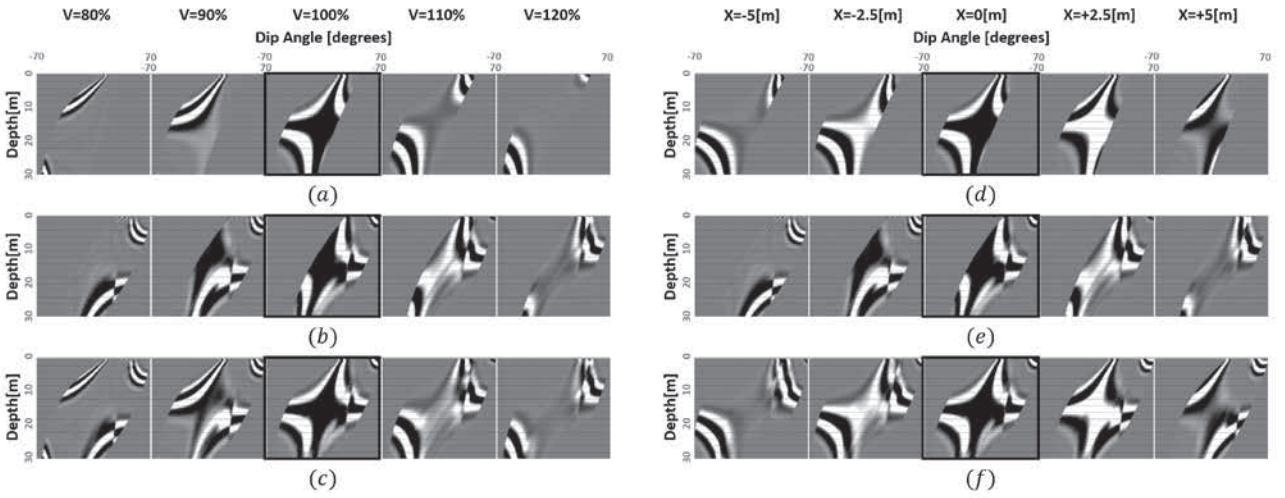

Figure 7 Dip angle gathers built from synthetic 2D data. (Left column) Data migrated with different velocities at the correct image point: (a) surface data; (b) vertical data; and (c) surface + vertical data. (Right column) Data migrated at different image points with the correct velocity: (d) surface data; (e) vertical data; and (f) surface + vertical data. From this example, one can see the high sensitivity of the dip angle gathers to positioning/velocity model errors.

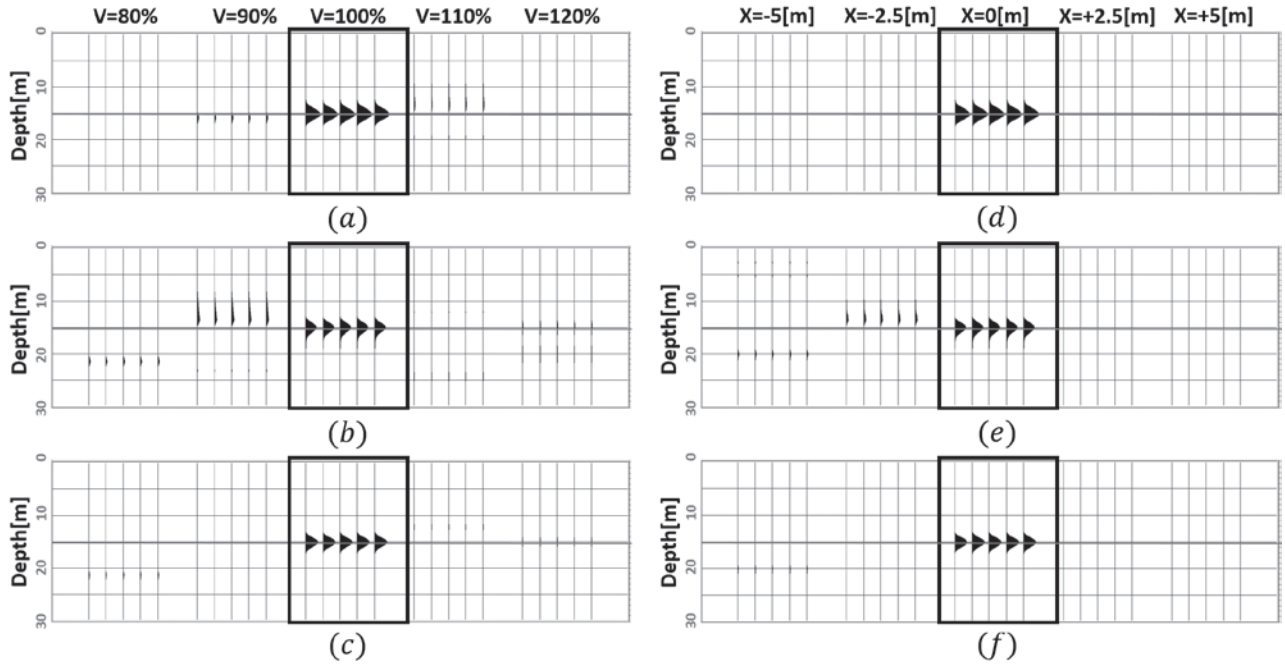

Figure 8 Semblance measure of the gathers shown in Figure 7. The semblance trace (between 0 and 1) is repeated five times. At the correct velocity and location combination, the highest semblance value is achieved at the correct depth (marked line).

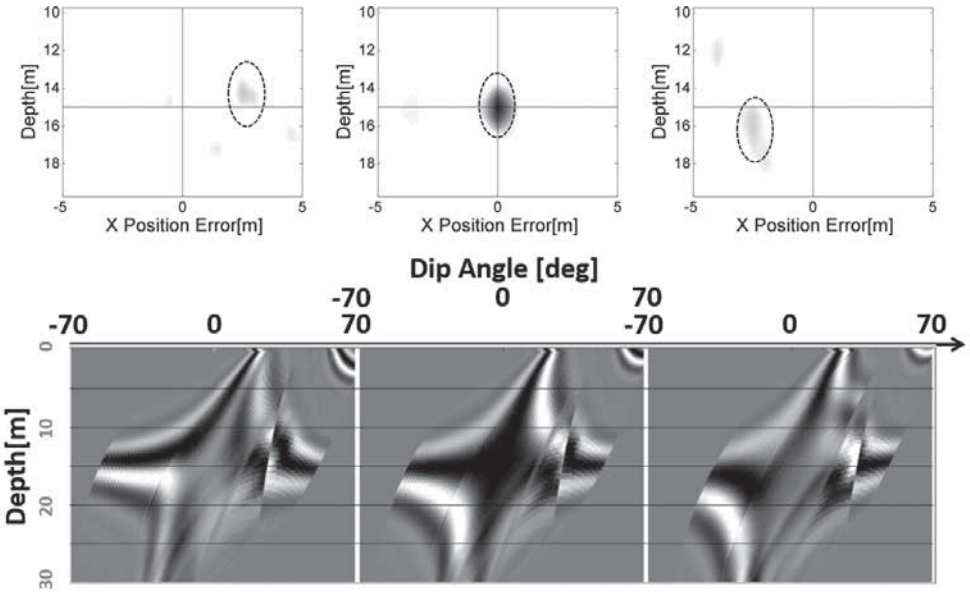

Figure 9 (Top) Coherency maps obtained using different velocity models - 90% (Left), 100% - correct (Middle), 110% (Right). At the correct velocity, the obtained image has a high coherency, and its centre is at the correct spatial location (denoted by the cross' centre). When a wrong velocity model is used, the image has low coherency, and its centre is shifted in both depth and X location. (Bottom) Dip angle gathers generated at the point of highest coherence value (encircled) for each velocity model. When a wrong velocity model is used, even the maximal semblance point does not arise from a flat moveout of the event.

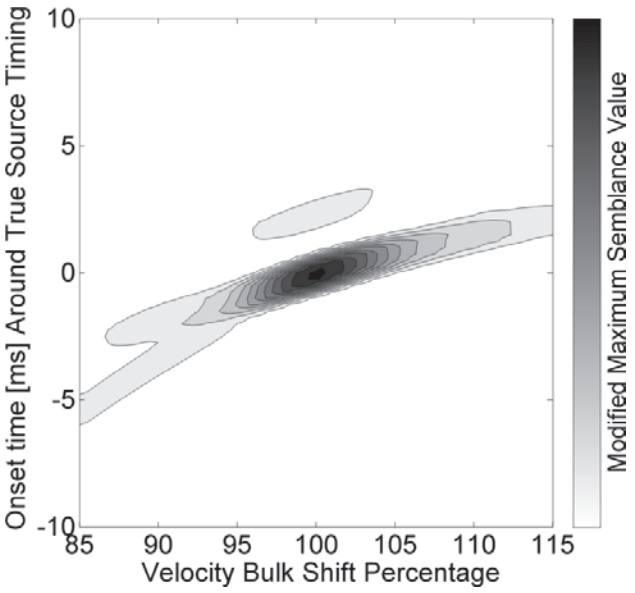

Figure 10 Onset time and velocity model search at the correct imaging point, using a combination of surface and vertical receivers. The highest coherence value (per gather) as a function of velocity model and source onset time is displayed. The maximal coherence is obtained at the correct velocity model and onset time. This maximal value was found at a depth of 15 m, as expected.

sition case. Thus, we are also able to show how a semblance-type measure, unaffected by the spurious solution, can be used to automatically choose the optimal migration velocity by measuring the migrated events' coherence. In order to avoid weak stretch effects being interpreted as coherent, we multiply the semblance by the mean value (or stack) of the gathers and thus assure that only the central, energetic part of the event is analysed. This procedure will be referred to as modified semblance measurement for the rest of this paper. Moreover, this figure demonstrates the uselessness of surface data if limited to a long (above 20 m) distance from the source as the event's moveout cannot be followed as velocities change, and as for real data cases, the covered dip range will not be sufficient to distinguish between different velocities in a coherence-based analysis. Gathers built from surface and vertical receivers' data as well as a combination of them are shown in Fig. 7 with their matching modified semblance measure in Fig 8. These figures show that the combined dip angle coverage is clearly larger than for surface data only (particularly if we were to limit it to long distance exclusively, as shown in Fig. 6). Moreover, surface and vertical data can be combined to a coherence-based analysis sensitive to both velocity and image location despite the non-conventional moveout of the migrated event in the gathers. Such an analysis is fully automatic and does not require any human interpretation of the gathers. It is also important to note that the expected polarity reversal of the data was corrected through knowledge of the incidence angles of rays reaching the receivers (not to be confused with their dip angle). If this angle was above 90°, the relevant trace was inverted.

Once gathers are built for all possible spatial imaging locations, one can measure their modified semblance (as shown in Fig. 8) and choose the most coherent imaging point as the best source location estimation. The result of applying this procedure on the combined vertical and surface data is shown in Fig. 9. When the correct velocity is used, the point of maximal semblance is at the true subsurface location. In addition to that, its value is significantly higher than the maximal coherence achieved when a wrong velocity model is used. This can also be seen by inspecting the gathers yielding the points of maximal coherence for different velocity models, i.e., only when the correct one is used the gather yielding the maximal coherence contains a flat moveout of the migrated event.

So far, we have assumed that the source onset time is known. However, this is not the case in reality. Therefore, one also needs to search for the source onset time using the migrated event's moveout as the objective function. The velocity and onset time are coupled but only to a certain extent. Whereas onset time shifts affect all receivers in the same way, a velocity bulk shift will translate to a different travel time shift in each receiver as the travel time from source to receiver is different. Therefore, this joint effect can be decoupled as we will show later, despite being only a higher order correction. In practice, this is done by detecting the overall first arrival time, i.e., the earliest time of arrival of all traces, using a multi-window auto-picking algorithm. Afterwards, we define a time window in which the source could have been excited—for the relevant configuration, between the overall first time of arrival and about 50[*ms*] before it is a good choice. This window arises from the relevant detection range of interest, which is in the few tens of meters, and the average P-wave velocity along the source–receiver path, which is about 1,000 m/s. Therefore, the travel time to the

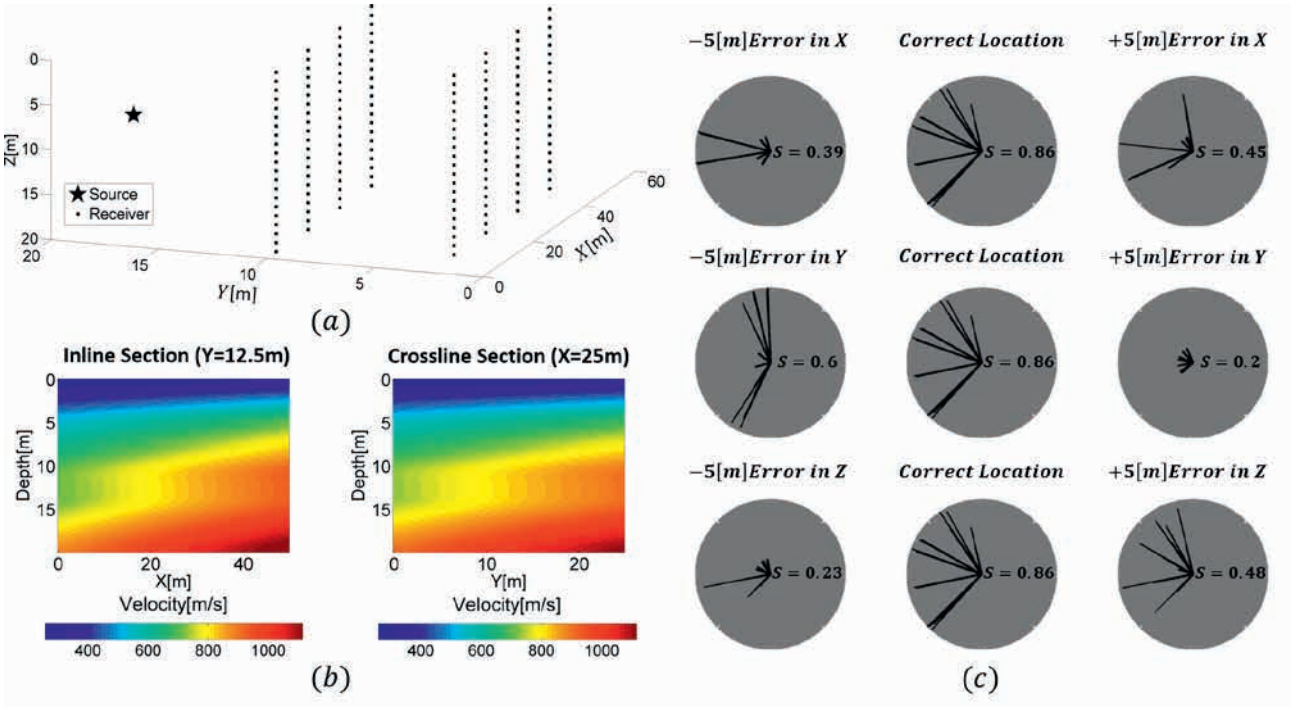

Figure 11 3D synthetic test: (a) Geometrical setup; (b) Representative inline and cross-line P-waves velocity model (for modeling and migration). For modeling, a constant V_p / V_s ratio of $\sqrt{3}$ was used. Notice the large depth variation (almost 300% over the depth range) superimposed on lateral variation. (c) Azimuthal gathers built at different locations, using the correct velocity model. Notice that, at the correct location (middle column), the semblance is high in all azimuths, whereas for wrong imaging points, the average value deteriorates (despite certain azimuths still holding high semblance values).

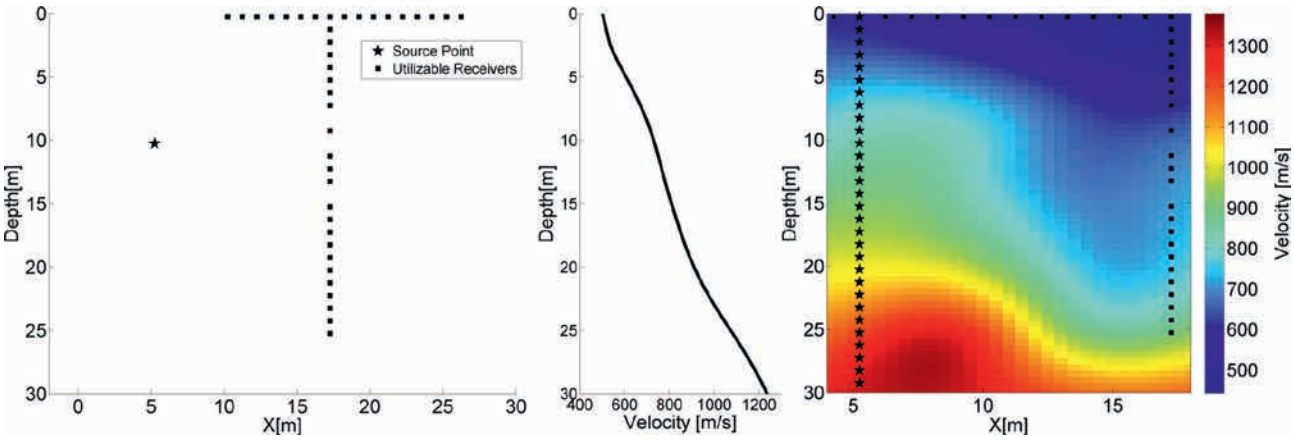

Figure 12 (Left) 2D cross-well experimental setup, (Middle) regional 1D model from check shots, and (Right) full tomography model. Note that the significant lateral variations of the full tomography model.

first receiver is bounded by their ratio, a few tens of milliseconds, and 50[*ms*] is a safe choice for the studied scenario but will vary in different cases. Within this time window, a different gather is built for every possible source onset time. For such a gather, the modified semblance is measured and retained. The result of such an analysis for different velocity models is shown in Fig. 10. In this example, we use a combination of surface and vertical receivers and perform the analysis at the correct imaging location. The obtained coherence is maximal within a certain region that encapsulates the coupling between velocity bulk shift and onset time previously discussed. However, this region (and accordingly, our error range) is quite limited and in this case, choosing its maximum yields the correct onset time and velocity. In addition, it is very important to state that when using surface receivers only such an analysis fails due to the coupling between depth, velocity, and onset time. The addition of vertically positioned receivers breaks the discrepancy by constraining the source's depth, hence yielding the correct solution as shown in Fig. 10. Conducting the same analysis at wrong imaging locations yields lower coherency values, thus indicating localization is possible without onset time knowledge.

Let us now move to a 3D example. The simulative setup, emulating a realistic acquisition setup, consists of various vertical arrays recording the signal (see Fig. 11a). The reasoning behind such a configuration is that since the velocity model (see Fig. 11b) varies much more in depth than in the lateral plane $\left(\{x, y\}\right)$, a finer sampling is needed in the former. This setup yields better coverage in dip (derived from receivers in depth) than azimuth (derived from receivers in the $\{x, y\}$ plane), and it is therefore more natural to choose working on a dip angle gathers for each azimuth. With this choice, we will have a few azimuths along which dip angle gathers will be built. However, each one of them will migrate a relatively large amount of data (a single vertical array at least) and therefore can be reliably analysed. Thus, for every imaging point in space $\left(\{x, y\}\right)$, one can measure the modified semblance along each of the azimuths and display it in a polar plot. This is equivalent to building a dip angle gather for every azimuth, measuring its modified semblance, and plotting its value at a given depth in all azimuths. Such plots are shown in (Fig. 11(c)). Only when built at the correct spatial location the semblance is high in all directions. Given any error in the estimated location of the source, whether in x,y or z, the average semblance value will be lower, despite possibly being high in certain azimuths. This type of analysis is a simple and intuitive way of localizing the source. As we also hold the original dip angle gathers, one can, albeit not necessarily, manually inspect the gathers that yielded those coherence values and estimate their quality.

SUGGESTED WORKFLOW

Before moving on to a real data example, we will briefly summarize the suggested workflow for a 2D case. The extension to 3D includes averaging the modified semblance along different azimuths and does not significantly change the workflow.

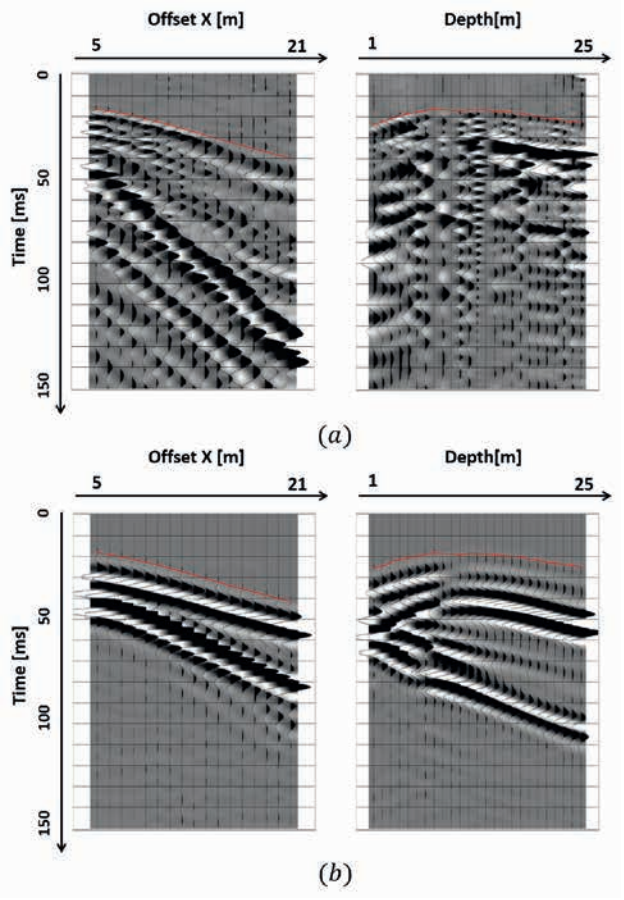

Figure 13 Field (a) and synthetic (b) recording of a source at 10[m] depth as recorded by surface line (left) and vertical array (right). Notice the excellent kinematic match (first break picking, in red, was conducted on the synthetic data before being applied to the real data with a bulk shift) between real and synthetic data as well as the expected polarity reversal of the first break of the vertical data.

For every possible imaging point, calculate, using ray tracing, the dip angles and travel times of the rays connecting image point and receivers.

For each imaging point, migrate the data into dip angle gathers and apply a modified semblance measure.

Repeat that process using different onset times (shifting the calculated travel times by a constant value) and different velocities (multiplying the calculated travel times by a certain percentage) and repeat step 2.

Find the maximum overall coherence in all possible combinations of imaging point, bulk shift of velocity model, and onset time. Its spatial location is the best estimation of the source location.

Optionally, inspect the gather that yielded the maximal coherence and examine it to assert the quality of the result.

REAL DATA EXAMPLE

A 2D cross-well operation was conducted. The source was a triggered downhole tool used in a cemented, cased borehole, and a

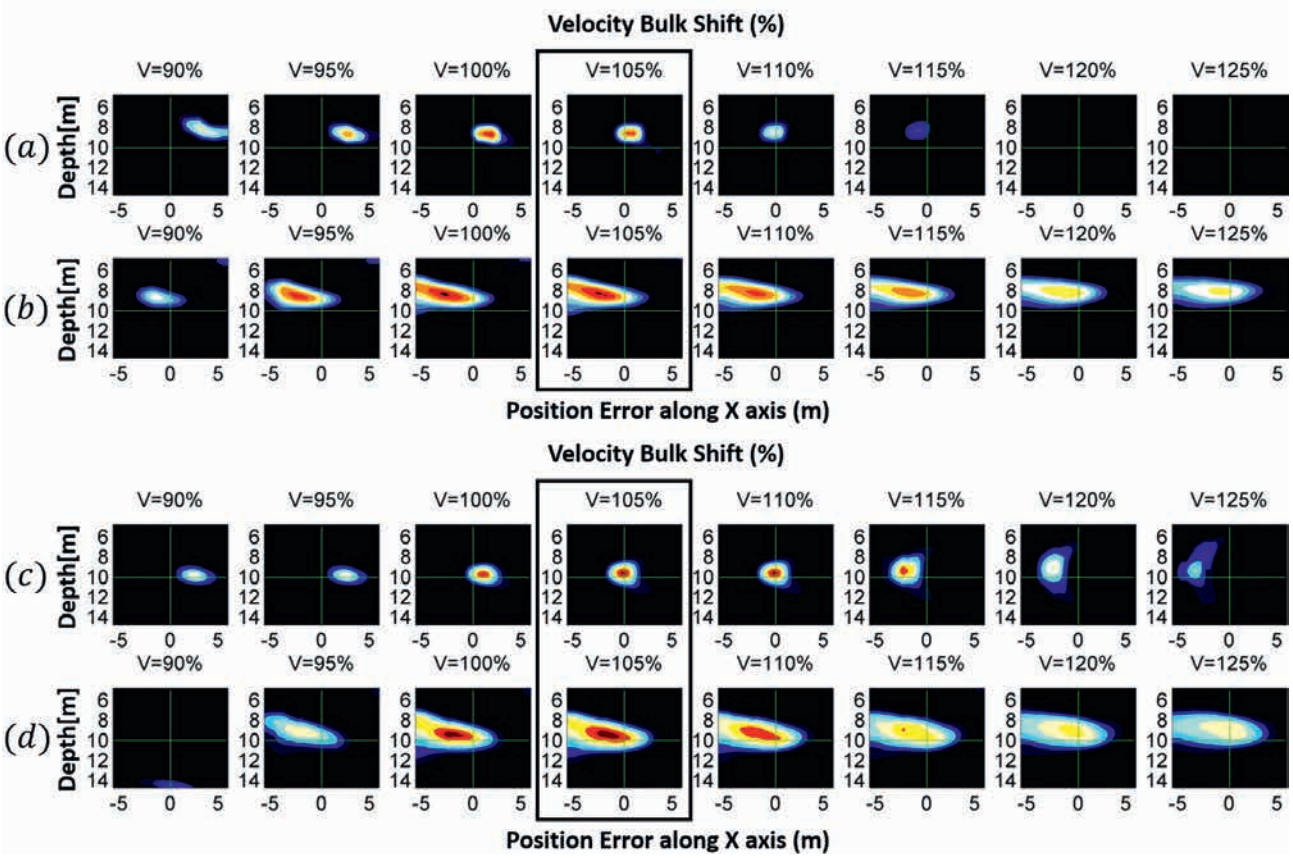

Figure 14 Source imaging using a 1D regional model with (a) and without (b) knowledge of the source onset time followed by imaging using the full tomography model with (c) and without (d) knowledge of the source onset time. The correct source location is at the cross centre. When the 1D model is used (a), the image is focused with a localization error arising from the velocity model only. When the onset time knowledge is removed (b), the image is smeared, and its maximal coherence, occurring at 105% of the initial velocity model, is located about 2.5m off in X and 1.5m off in Z. When the full tomography model is used (c), there is a very small to non-existent localization error due to the velocity model. When the onset time knowledge is removed (d), the maximal coherency point (obtained again at 105% of the initial model) has a significantly smaller localization error than (b), thus indicating the superiority of this velocity model.

buried array of geophones was set up in a borehole about 12 m away from it, covering depths of 1 m–30 m. The experimental setup was completed with surface receivers, as shown in Fig. 12 (left). As explained, the localization procedure requires a certain background velocity model. It is important to note that we assume an isotropic, deterministic medium, which is only an approximation of the subsurface. However, for practical reasons and lack of more detailed knowledge, we elect to focus on using the best possible P-wave velocity model knowing that this could possibly induce certain errors in the process. For this study, a cross-hole survey, mixed with surface receivers, was also conducted in the area of interest. Using the first break picks and a travel-time tomography procedure, the optimal velocity model was built. This is important both as a reference point in analysing our workflow and as a representing case in which, despite acquisition from offset, one has detailed knowledge of the velocity field. However, for realistic scenarios that do not allow for such prior knowledge, a regional 1D simplified velocity model was also extracted from check shots, also known as zero-offset vertical seismic profile (Fig. 12, right and middle, respectively). For practical scenarios, where localization from offset is required, this is the model quality one can expect. A comparison between field and synthetic data (created using the full tomography model) is shown in Fig. 13, showing the excellent kinematic match of the first break between the two datasets.

Let us now localize the source using both the regional 1D and full tomography model, as well as with and without knowledge of the source onset time. For both cases, imaging will be performed with different velocity bulk shifts. When an onset time search is performed, the maximal obtained modified semblance is displayed. Figure 14 compiles the results of this analysis. First of all, it can be seen that, even when using the regional velocity model and without knowledge of the onset time (b), a relatively precise localization is possible, thus indicating the usefulness of the method. When the full tomography velocity model (d) is used, localization results significantly improve. The difference

between (a) and (c) clearly shows the superiority of the full tomography model as it yields a more precise localization when the onset time doesn't affect the results. Localization error margins can be estimated from coherency contours in (b) and (d) and are limited to about $\pm 1.5m$ in X and $\pm 0.5m$ in Z.

It is also important to note that both models yielded optimal results when a certain bulk shift of the velocity (105%) was applied to them. Thus, the described basic velocity analysis procedure is necessary yet simple to implement. The reason for this is that the initial model was built using a tomographic procedure on a full survey, optimizing the inverted model for the entire dataset. However, in this example, we are analysing only a single source, thus making it possible that a higher/lower velocity model may be more adequate for this specific source.

CONCLUSIONS

Under the challenging conditions imposed by the shallow subsurface medium, conventional localization methods may not be suitable. A new imaging-based method for the localization of shallow seismic events was presented, utilizing the diffractive nature of the source. The method uses migration to the local angle domain where the source's contribution should be coherent in all angles. In this domain, the migration is correct in its physical sense, and artificial results due to acquisition geometry footprints are avoided. Then, a modified semblance criterion is applied on the migrated gathers and its maximum's position indicates the most probable source location. However, this criterion can and should also be used for velocity analysis. Automatically updating the velocity model is possible by applying bulk shifts in search for a maximal coherence measure. Of course, manually inspecting the gathers could lead to finer updates of the velocity model as our choice of CIG domain allows us to map each angle to a certain ray path, thus indicating the parts of the model that need updating.

Using extensive synthetic tests and a 2D field example, we have shown the usefulness of the dip angle gathers for both interval velocity analysis and source localization. The chosen field example was challenging due to a high inhomogeneous subsurface and a low amount of traces recorded from standoff. Despite that, a fully automatic procedure using regional knowledge of the velocity model combined with surface and vertically positioned receivers yields a relatively precise localization.

The importance of the initial velocity model is evident. Usage of an approximated model introduces localization errors even with a known source onset time. However, we have seen that transition from a regional 1D model to a full tomography model significantly improves localization results, both with and without knowledge of the onset time. In addition to that, for both models, the most coherent image was found at 105% of the initial velocity model. This indicates the need for the simple bulk shift velocity update procedure, which we suggested, even when using complex initial velocity models.

The usage of vertically positioned receivers is critical. First of all, without it, the unknown onset time makes it impossible to properly localize the source in depth. Second, surface-only data from standoff lacks dip angle coverage, as shown in synthetic examples. Furthermore, the usage of vertical arrays can greatly simplify the initial model building. By utilizing simple checkshot procedures, a good regional velocity model can be obtained, assuming no dramatic lateral variation occurs within the range of interest.

The transition to a 3D acquisition is required and expected to improve localization results. In addition to the usage of more data and a better velocity model, the multi-azimuth coverage is expected to yield a better positioning in the xy plane while maintaining the accuracy of depth positioning.

REFERENCES

Bai C.-Y. and Kennett B.L.N. 2000. Automatic phase-detection and identification by full use of a single three-component broadband seismogram. *Bulletin of the Seismological Society of America* **90**(1), 187–198.

Bai Y., Sun Z., Chen L., and Yang H. 2011. Seismic diffraction separation in 2D and 3D space. 73rd EAGE Conference & Exhibition, Vienna, Austria, May 2011.

Bardainne T. and Gaucher E. 2010. Constrained tomography of realistic velocity models in microseismic monitoring using calibration shots. *Geophysical Prospecting* **58**(5), 739–753.

Biondi B. 2006. *3D Seismic Imaging*. Society of Exploration Geophysicists.

Dafni R. and Reshef M. 2012. Interval velocity analysis using multiparameter common image gathers. *Geophysics* **77**(4), U63.

Earle P.S. and Shearer P.M. 1994. Characterization of global seismograms using an automatic-picking algorithm. *Bulletin of the Seismological Society of America* **84**(2), 366–376.

Komatitsch D. and Tromp J. 1999. Introduction to the spectral element method for three-dimensional seismic wave propagation. *Geophysical Journal International* **139**(3), 806–822.

Koren Z. and Ravve I. 2011. Full-azimuth subsurface angle domain wavefield decomposition and imaging Part I: Directional and reflection image gathers. *Geophysics* **76**(1), S1–S13.

Maxwell S. and Urbancic T. 2001. The role of passive microseismic monitoring in the instrumented oil field. *The Leading Edge* **20**(6), 636–639.

Ravve I. and Koren Z. 2011. Full-azimuth subsurface angle domain wavefield decomposition and imaging: Part 2 - Local angle domain. *Geophysics* **76**(2), S51–S64.

Reshef M., Lipzer N., Dafni R. and Landa E. 2012. 3D post-stack interval velocity analysis with effective use of datuming. *Geophysical Prospecting* **60**(1), 18–28.

Reshef M. and Rüger A. 2008. Influence of structural dip angles on interval velocity analysis. *Geophysics* **73**(4), U13.